Exclusion of Axionlike-Particle Cogenesis Dark Matter in a Mass Window above 100 μeV

Aaron Quiskamp,[1,*] Ben T. McAllister,[1,2,†] Paul Altin,[3] Eugene N. Ivanov,[1] Maxim Goryachev,[1] and Michael E. Tobar[1,‡]
[1]Quantum Technologies and Dark Matter Laboratory, Department of Physics, University of Western Australia, 35 Stirling Highway, Crawley, Western Australia 6009, Australia
[2]ARC Centre of Excellence for Dark Matter Particle Physics, Swinburne University of Technology, John Street, Hawthorn, Victoria 3122, Australia
[3]ARC Centre of Excellence For Engineered Quantum Systems, The Australian National University, Canberra, Australian Capital Territory 2600, Australia

(Received 3 October 2023; accepted 28 November 2023; published 16 January 2024)

We report the results of Phase 1b of the ORGAN experiment, a microwave cavity haloscope searching for dark matter axions in the 107.42–111.93 μeV mass range. The search excludes axions with two-photon coupling $g_{a\gamma\gamma} \geq 4 \times 10^{-12}$ GeV^{-1} with 95% confidence interval, setting the best upper bound to date and with the required sensitivity to exclude the axionlike particle cogenesis model for dark matter in this range. This result was achieved using a tunable rectangular cavity, which mitigated several practical issues that become apparent when conducting high-mass axion searches, and was the first such axion search to be conducted with such a cavity. It also represents the most sensitive axion haloscope experiment to date in the ∼100 μeV mass region.

DOI: 10.1103/PhysRevLett.132.031601

Although direct detection remains elusive, cosmological observations and early Universe simulations allow us to indirectly infer the presence of dark matter, which is thought to constitute ∼85% of the total matter and ∼27% of the total energy density in our Universe [1]. The axion particle is one of the most compelling candidates for dark matter and was originally postulated by Peccei and Quinn as a solution to the strong CP (charge-parity) problem in quantum chromodynamics (QCD) [2–4].

Axions can be detected using a kind of experiment called a resonant cavity haloscope, first proposed by Sikivie, by exploiting their expected coupling to electromagnetism [5,6]. When immersed in a strong dc magnetic field, axions are expected to create detectable photons via the inverse Primakoff effect, with a frequency $\nu_a = m_a c^2/h + \mathcal{O}(10^{-3}c)$, where m_a is the axion rest mass and $\mathcal{O}(10^{-3}c)$ is the expected velocity dispersion that results in an effective axion quality factor Q_a [7,8]. Tuning the resonant cavity to this frequency enhances the signal by the cavity quality factor Q_0. However, because the axion mass and the axion-photon coupling $g_{a\gamma\gamma}$ are unknown, a wide parameter space spanning several orders of magnitude must be scanned. Although unconstrained by theory, most models favor an axion with a mass above $\mathcal{O}(\mu\text{eV})$ [9–11] and below $\mathcal{O}(\text{meV})$ [12,13].

For example, the standard model axion seesaw Higgs portal inflation (SMASH) model is a well-motivated description of particle physics that predicts axion dark matter particles to have mass 50 μeV $\leq m_a \leq$ 200 μeV [14,15]. The Kim-Shifman-Vainshtein-Zakharov and Dine-Fischler-Srednicki-Zhitnitsky models are two of the most popular QCD axion models and are parametrized by the dimensionless coupling constant g_γ, taking values of −0.97 and 0.36, respectively [16–20]. Together with the axion decay constant f_a, and the fine structure constant α, they determine the axion-photon coupling $g_{a\gamma\gamma} = \alpha g_\gamma/\pi f_a$. The axion converted photon power at these couplings is extremely weak $\sim\mathcal{O}(10^{-22}$–10^{-23} W), and only two experiments so far have attained the required sensitivity: ADMX [21–24] and CAPP-12 TB [25].

The expected axion-photon signal power on resonance extracted by the haloscope is given by [26]

$$P_{a\to\gamma} = \left(g_{a\gamma\gamma}^2 \frac{\rho_a}{m_a}\right)\left(\frac{\beta}{1+\beta} B_0^2 V C Q_L\right). \tag{1}$$

Here, $\rho_a \approx 0.45$ GeV/cm^3 is the local dark matter density (assumed to be all axions), β is the coupling of the "strongly" coupled antenna port to the haloscope, Q_L is the resonator loaded quality factor, V is the cavity volume, and C is the form factor which represents the degree of overlap between the cavity electric field and the externally applied magnetic field, with field strength B_0.

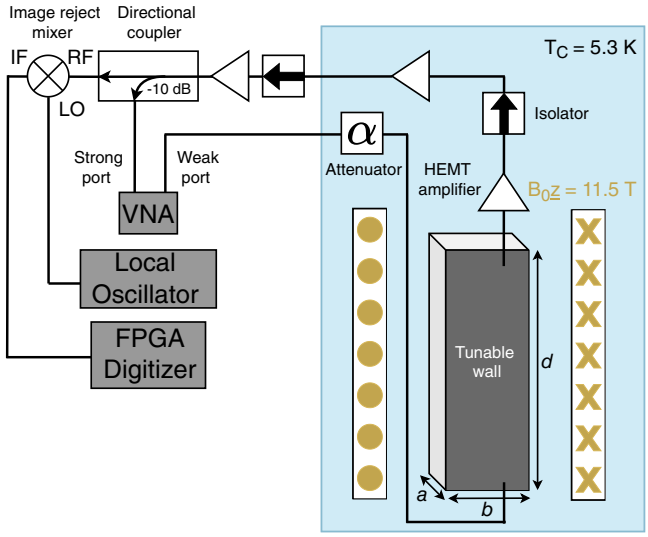

FIG. 1. A diagram of the ORGAN Phase 1b experiment. The rectangular cavity at physical temperature $T_C = 5.3$ K with dimensions a, b, and d as mentioned in the text is placed inside a solenoidal magnet (gold) with a field strength of 11.5 T. The tunable wall is shown shaded in dark gray. An expected axion signal would first be amplified through a series of HEMT amplifiers and later mixed down to an intermediate frequency (IF) using an image rejection mixing stage and local oscillator (LO) for sampling by a field-programmable gate array (FPGA) digitizer. The frequency response of the TM_{110} mode in transmission is measured using a vector network analyzer (VNA).

The oscillating resonant group axion (ORGAN) experiment is a microwave cavity haloscope hosted at the University of Western Australia which targets its search for axions in the 62–207 μeV (15–50 GHz) mass region, encompassing the majority of the predicted SMASH range [27,28]. Phase 1a of ORGAN was recently completed, scanning over the mass range between 63.2–67.1 μeV and setting an upper limit on axion-photon couplings $|g_{a\gamma\gamma}| \geq 3 \times 10^{-12}$ in this range [27]. This search was sufficient to exclude the axionlike particle (ALP) cogenesis model, which is another well-motivated model that predicts much stronger axion-photon coupling than QCD axion models [29–31].

In this work, we report the results of the ORGAN Phase 1b experiment (depicted in Fig. 1), which achieves ALP cogenesis exclusion over the 107.42–111.93 μeV (25.97–27.07 GHz) mass range, while operating at a physical temperature of ∼5.3 K and in an 11.5-T magnetic field. First-stage amplification is achieved using a low-noise high electron mobility transistor (HEMT) amplifier, which is directly connected to the strongly coupled port of the cavity for negligible loss.

The signal-to-noise ratio (Σ) of a haloscope to a given [32],

$$\Sigma = \frac{P_{a\to\gamma}}{k_B T_{\mathrm{sys}}} \sqrt{\frac{\tau}{\Delta\nu_a}}, \tag{2}$$

where k_B is Boltzmann's constant, T_{sys} is the total system noise temperature, τ is the integration time, and $\Delta\nu_a = \nu_c/Q_a \sim \nu_c/10^6$ is the expected axion linewidth given by the isothermal, virialized halo model for axion dark matter [7,8]. The total system noise temperature is thus a critical parameter in haloscope sensitivity. In Phase 1b, similarly to Phase 1a, we express the total system noise as [33],

$$T_{\mathrm{sys}} = T_C \frac{4\beta}{(1+\beta)^2 + 4\Delta^2} + T_A \frac{1+4\Delta^2}{(1+\beta)^2+4\Delta^2}. \tag{3}$$

Here, T_A is the added noise from the first stage amplifier (the contribution to the total added noise from subsequent amplification stages is suppressed by the first stage gain and so can be safely ignored), T_C is the physical cavity temperature, and $\Delta = (\nu - \nu_c)/\Delta\nu_c$ is the detuning from resonance normalized to the cavity linewidth $\Delta\nu_c$. It should be noted that the first stage amplifier is oriented parallel to the applied magnetic field to avoid negative effects on amplifier gain and noise figure [34].

To date, the most sensitive searches have primarily utilized cylindrical tuning-rod-based resonators which employ a TM_{010} mode. Such resonators are capable of maximizing $B_0^2 V$ in typical, cylindrical solenoidal magnets, and these designs have achieved state-of-the-art sensitivity in the mass range around a few μeV. However, this type of design is subject to significant challenges, particularly in the move to higher axion masses (and equivalently higher resonant frequencies). Challenges such as tuning rod misalignment and sticking at cryogenic temperatures (reducing C and Q_0), radiation leakage as a result of external mechanical tuning (reducing Q_L), and poor tuning rod thermalization (increasing T_{sys}) can occur in these resonators and are common experimental hurdles. These factors together dramatically degrade the achievable scan rate. For these and other reasons, alternate experimental approaches have been proposed—including dielectric and multicell haloscopes, and other designs [35–39].

In ORGAN Phase 1b we opt for a different style of resonator in an attempt to mitigate the challenges above, some of which are expectedly amplified in the high frequency regime owing to the necessarily small volume. A rectangular oxygen-free-high conductivity copper cavity was chosen, where the axion-sensitive TM_{110} mode was tuned by moving a single cavity wall perpendicular to the B^z field direction. The cavity dimensions of $a = 5.6$–6 mm in the tunable $\vec{x}$ direction, $b = 27.1$ mm in the $\vec{y}$ direction, and $d = 77.3$ mm in the $\vec{z}$ direction were chosen such that no mode crossings occur in the targeted 26–27 GHz scan range. The electric field profile for the TM_{110} mode with the chosen cavity dimensions is shown in Fig. 2. Although this design suffers some volume loss when compared to a cylindrical tuning-rod-based resonator, it can be partially or fully compensated by the increased form factor, with $C_{110} = 0.65$. Furthermore, the straightforward frequency

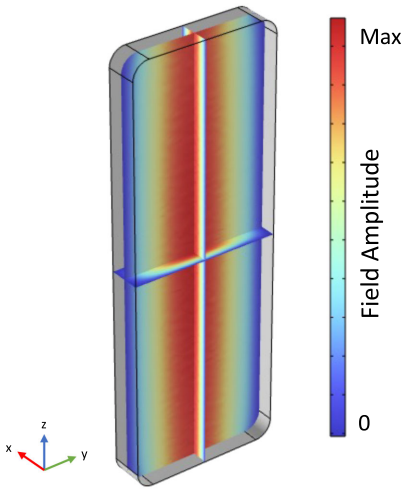

FIG. 2. An isometric view of the z component of the TM_{110} electric field. The resonant frequency of the rectangular cavity is tuned via the movement of one of the sidewalls.

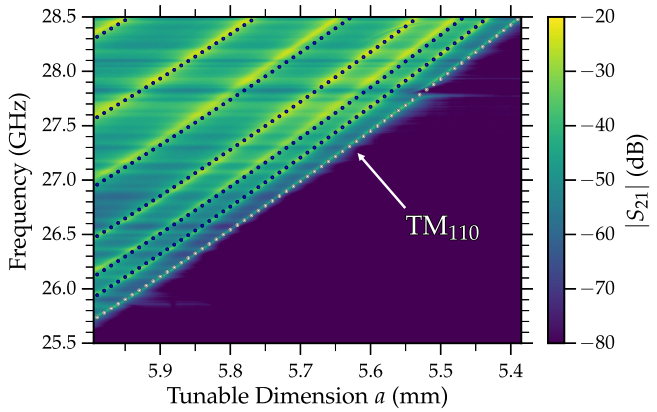

FIG. 3. A color density plot of the transmission coefficient $|S_{21}|$ (decibel) as a function of frequency and tunable cavity dimension a. The axion-sensitive TM_{110} mode is annotated and tunes over the targeted 26–27 GHz range with no mode crossings. The broad horizontal lines represent standing waves in the cavity-receiver chain. The dots represent COSMOL modeling of the TM_{110} mode (white) and the first six TM_{11p} modes (blue).

tuning mechanism in the form of a movable wall which is only required to move a fraction of a millimeter within the cavity reduces complexity, which is critical at cryogenic temperatures. The design also maintains good thermalization as no weak link to the tuning mechanism is required. Additionally, the absence of a tuning rod minimizes longitudinal symmetry breaking and avoids the introduction of transverse electromagnetic modes. This results in a reduction in both the strength and number of mode crossings, which are regions of orthogonal mode hybridization preventing axion-sensitive data from being taken here. Further details of this haloscope design, particularly in comparison with the standard tuning-rod haloscope, can be found in [40].

ORGAN Phase 1b acquired data for ~28 days including rescans, covering all axions masses between 107.42–111.93 μeV (25.97–27.07 GHz) with sufficient sensitivity to exclude the ALP cogenesis model over the entire range. Again, there were no mode interactions in the range, and thus no forbidden frequencies. The strong port coupling was set statically and characterized in a dedicated cooldown and experimental run before data taking, which when combined with Q_L measurements gave an estimate of the intrinsic quality factor Q_0. Using this mapping between Q_L, ν_c, and β, the antenna coupling for the data-taking run can be inferred at each cavity position directly from the *in situ* measurement of Q_L. Throughout the scan, Q_L had a typical value of ~3700, and β was found to lie between 0.19–2.18 with a mean value of 1.22. The average deviation in Q_L, and the subsequently interpolated β values at a given cavity frequency between the two cooldowns, were 4.6% ($\sigma = 2.5\%$) and 8.8% ($\sigma = 5.2\%$), respectively. As such, we can estimate the coupling to within a tolerable uncertainty without the need to measure it directly *in situ*.

As discussed, frequency tuning was achieved by moving a single cavity wall in the $\vec{x}$ direction via an Attocube ANPz101 piezoelectric stepper motor mounted externally to the cavity. The tunable wall had 0.1 mm gaps between all four sides of the wall and cavity, allowing consistent and repeatable tuning at cryogenic temperatures. To mitigate the substantial radiation leakage introduced by the gaps, a quarter-wavelength rf choke was cut into all four narrow sides of the tunable wall. Because the physical cavity dimensions were changed to tune the resonant frequency, so too was the volume, which for the frequency range scanned varied between 11.8 and 12.3 mL.

The tunable copper wall was thermalized to the copper cavity through the titanium Attocube stepper motor via a copper mounting plate. Thermalization was experimentally verified by placing a temperature sensor at the top of the cavity and on the tuneable wall in a separate cooldown. Notably, no temperature gradient was observed between the wall, cavity, and 4K plate even when stepping the motor.

The form factor C was calculated to be ~0.40 using finite element method modeling in COMSOL Multiphysics. The reduction in C compared to the theoretical maximum value of ~0.65 for this cavity geometry arises from tilt in the tunable wall. The degree of tilt was quantified by minimizing the measured frequency deviations between the TM_{11p} mode family and theoretical modeling in COMSOL, which is displayed in Fig. 3. By considering tilt of the wall in the $\vec{x}$ direction, we find the minimum average deviation between the first six TM_{11p} ($p \geq 1$) modes to be 0.087%, which occurs when the degree of tilt from vertical is ~0.067°. In principle, this tilt can be mitigated through enhanced mechanical design, for example, ultralow run-out stepper motors, lighter tunable walls, and improved assembly tolerances. Such adjustments are planned for future searches. We believe that the degree of tilt can be reduced to less than ~0.02°, corresponding to $C \geq 0.58$ with these

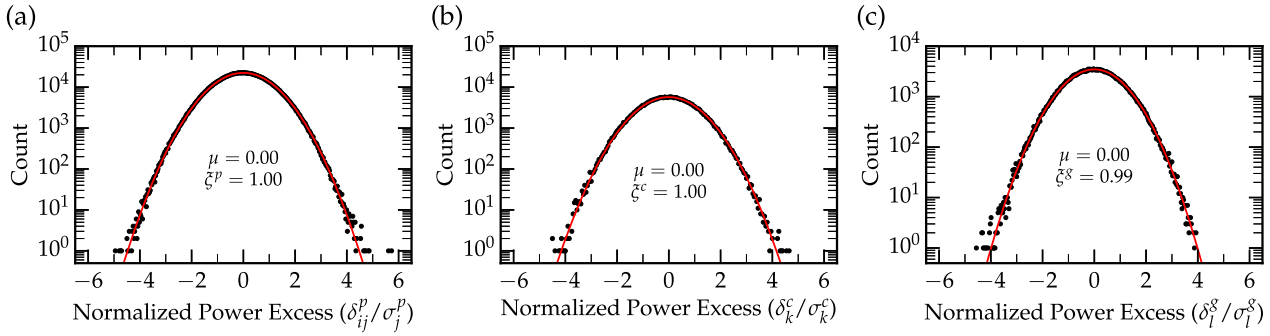

FIG. 4. Distributions of the normalized power excess from all frequency bins (black circles) are shown at different stages of the coadding procedure, with the corresponding Gaussian fits (solid red). (a) Normalized excess power in the jth bin of the ith SG filtered spectrum δ^p_{ij}/σ^p_j shows the expected Gaussian distribution with $\mu = 0$ and width $\xi^p = 1$. (b) The normalized excess power in the kth vertically combined bin is given by δ^c_k/σ^c_k, and preserves the Gaussian noise with $\mu = 0$ and $\xi^c = 1$. (c) The distribution of normalized grand spectrum bins δ^g_l/σ^g_l after the horizontal coaddition and optimal filtering deviates from the standard normal Gaussian distribution with a reduced width $\xi^g = 0.99$. This results from the negative correlations between adjacent coadded bins that are induced by the SG filter.

improvements. However, it should be noted that the degradation in C due to wall tilt is dependent on the wall position since an equivalent degree of tilt has a greater relative effect with decreasing cavity dimensions.

The readout chain, as shown in Fig. 1, consisted of a vector network analyzer (VNA) that measured the frequency response of the TM_{110} mode in transmission to find Q_L, ν_c, and $\Delta\nu_c$ at each tuning step. After the first amplification stage, isolators were used between stages to prevent backaction noise. The down-mixing stage achieved image rejection of the noisy, amplifier-only sideband by driving two identical mixers with the same local oscillator (LO) source except 90° out of phase. The intermediate frequency (IF) outputs from both mixers were recombined using a 90° hybrid coupler and sampled by a 250 MS/s digitizer (NI-5761R) with real-time data processing done on a field-programmable gate array (FPGA; Xilinx Kintex-7, NI-7935R). A zero dead-time, hybrid superheterodyne fast Fourier transform spectrum analyzer was implemented on the FPGA, generating a 6553 point, 25-MHz-wide spectrum centered at 45 MHz, with a bin width of $\Delta\nu_b \approx 3815$ Hz. This center frequency was carefully chosen to avoid unwanted low-frequency interference and the appropriate low-pass filter attenuated any spurious high-frequency interference. The analysis window was then cropped to be 9.91 MHz wide to avoid harmonics of the 10 MHz reference clock signal at 40 and 50 MHz.

The integration time at each cavity frequency varied between 38 and 211 min and was adjusted based on V, Q_L, and β to maintain sensitivity better than the ALP cogenesis model bands. The data analysis procedure follows the method outlined by the Haloscope at Yale Sensitive to Axion CDM (HAYSTAC) experiment [41], and is the same method used in the ORGAN Phase 1a analysis [27]. The slowly varying baselines of the raw power spectra are removed with a Savitsky-Golay (SG) filter while preserving spectral features on the scale of $\Delta\nu_a \sim 26$–27 kHz, which equates to $\sim 7\Delta\nu_b$ for this search. The SG filter had a polynomial degree of 5 and a 401-point window size. However, the SG filter is known to attenuate potential axion signals as a result of its imperfect stop band attenuation [41]. Through simulation, we find the attenuation of an axion signal due to SG filtering to be $\eta_{\mathrm{SG}} = 0.95$, which reduces our exclusion power by the same factor. After normalizing via the SG filter and subtracting 1 so that the spectra have $\mu = 0$, we obtain a set of dimensionless, normalized excess power spectra and in the absence of axion conversion, each bin is a Gaussian random variable with $\mu = 0$ and standard deviation $\sigma^p = 1/\sqrt{\Delta\nu_b \tau}$. The processed spectra are subsequently rescaled according to their expected axion sensitivity such that overlapping spectra can be vertically combined using a maximum likelihood weighted sum which maximizes Σ. However, as mentioned the axion line shape is expected to follow a Maxwell-Boltzmann distribution and so bins must be coadded horizontally to match this width and shape. We enhance our sensitivity to axion detection by optimally filtering sets of seven consecutive bins according to this expected line shape, resulting in a normalized "grand power spectrum" which is shown as a histogram in Fig. 4. A rescan threshold of 4σ was set, which five spectra exceeded.

The potential axion candidates were rescanned with sufficient integration time so that after subjecting the rescanned spectra to analysis, none were found to still exceed the 4σ threshold. A 95% confidence level (C.L.) is chosen and corresponds to an Σ target of 5.645σ, from which an upper bound on axion-photon coupling is set, assuming axions make up 100% of the local dark matter density of 0.45 GeV/cm^3. As shown in Fig. 5, ORGAN Phase 1b surpasses the limits set by the CERN axion solar telescope (CAST) [42] by over an order of magnitude and excludes ALP cogenesis over the targeted mass range of 107.42–111.93 μeV (25.97–27.07 GHz). The "notch" at

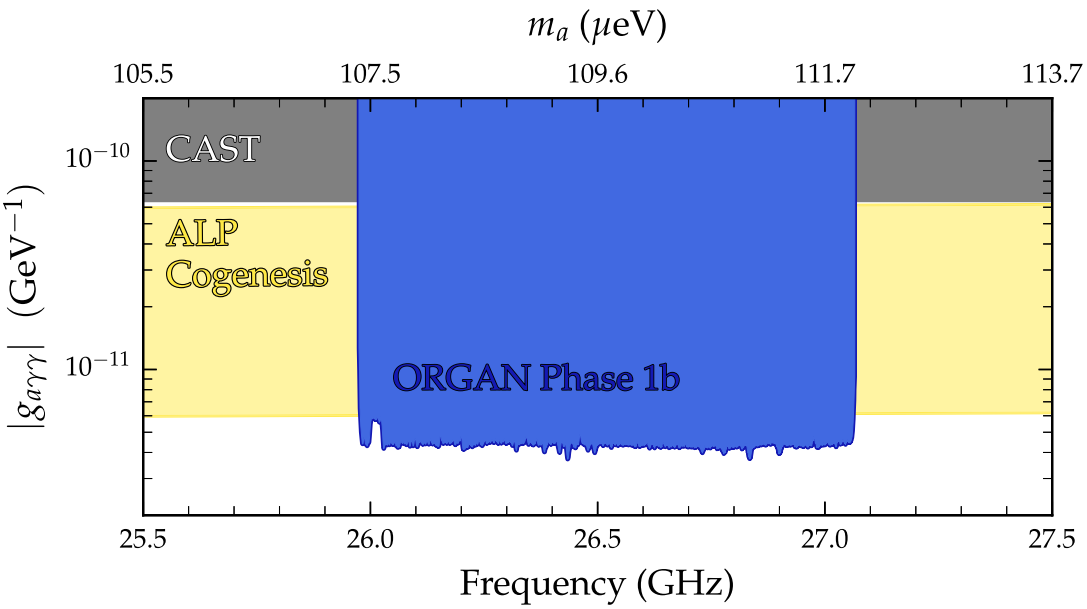

FIG. 5. The upper exclusion limits on $g_{a\gamma\gamma}$ from ORGAN Phase 1b at a 95% C.L. is shown shaded in blue. Previous limits set by CAST (gray) [42] and ALP cogenesis model band (yellow) [29–31] are also shown. The notch at ~26 GHz is due to insufficient integration time in this region.

26 GHz is due to insufficient integration time early in the data-taking run, but the sensitivity is still sufficient to exclude ALP cogenesis in this region. We calculate the fractional uncertainty on axion-photon coupling in the same way as ORGAN Phase 1a [27], which takes into account uncertainties in the parameters $\beta(8.8\%)$, $Q_L(4.6\%)$, $C(5\%)$, $V(1\%)$, and $T_A(10\%)$. This results in a total uncertainty of $\delta g_{a\gamma\gamma} \approx 6.4\%$.

We have reported on Phase 1b of the ORGAN experiment, a high-mass axion haloscope hosted at the University of Western Australia. Phase 1b excluded ALP cogenesis dark matter in the mass range of 107.42–111.93 μeV. With the completion of Phase 1b, the first phase of ORGAN is now complete, and to date has set the most sensitive limits on axion-photon coupling above 10.4 GHz (43 μeV) [43], excluding ALP cogenesis over the searched ranges. Phase 1b utilized a novel type of resonator, and has demonstrated the feasibility of high mass axion searches despite the unfavorable sensitivity scaling. Future phases will leverage detector and readout upgrades such as new cavity designs, gigahertz single photon counting, superconducting cavities, and a larger magnet to probe deeper into the parameter space between 15–50 GHz.

This work is supported by Australian Research Council Grants No. CE17010009 and No. CE200100008.

*aaron.quiskamp@research.uwa.edu.au
†ben.mcallister@uwa.edu.au
‡michael.tobar@uwa.edu.au

[1] P. A. R. Ade *et al.* (Planck Collaboration), Planck 2015 results—XIII. Cosmological parameters, Astron. Astrophys. **594**, A13 (2016).
[2] R. D. Peccei and H. R. Quinn, *CP* conservation in the presence of pseudoparticles, Phys. Rev. Lett. **38**, 1440 (1977).
[3] S. Weinberg, A new light boson?, Phys. Rev. Lett. **40**, 223 (1978).
[4] F. Wilczek, Problem of strong p and t invariance in the presence of instantons, Phys. Rev. Lett. **40**, 279 (1978).
[5] P. Sikivie, Experimental tests of the "invisible" axion, Phys. Rev. Lett. **51**, 1415 (1983).
[6] P. Sikivie, Experimental tests of the "invisible" axion, Phys. Rev. Lett. **52**, 695(E) (1984).
[7] M. S. Turner, Periodic signatures for the detection of cosmic axions, Phys. Rev. D **42**, 3572 (1990).
[8] R. Jimenez, L. Verde, and S. P. Oh, Dark halo properties from rotation curves, Mon. Not. R. Astron. Soc. **339**, 243 (2003).
[9] J. Preskill, M. B. Wise, and F. Wilczek, Cosmology of the invisible axion, Phys. Lett. **120B**, 127 (1983).
[10] P. W. Graham and A. Scherlis, Stochastic axion scenario, Phys. Rev. D **98**, 035017 (2018).
[11] R. R. Volkas, VISHν: Flavour-variant DFSZ axion model for inflation, neutrino masses, dark matter, and baryogenesis, Lett. High Energy Phys. **2023** (2023).
[12] J. Preskill, M. B. Wise, and F. Wilczek, Cosmology of the invisible axion, Phys. Lett. **120B**, 127 (1983).
[13] W. Keil, H.-T. Janka, D. N. Schramm, G. Sigl, M. S. Turner, and J. Ellis, Fresh look at axions and SN 1987A, Phys. Rev. D **56**, 2419 (1997).
[14] G. Ballesteros, J. Redondo, A. Ringwald, and C. Tamarit, Unifying inflation with the axion, dark matter, baryogenesis,

and the seesaw mechanism, Phys. Rev. Lett. **118**, 071802 (2017).
[15] G. Ballesteros, J. Redondo, A. Ringwald, and C. Tamarit, Several problems in particle physics and cosmology solved in one smash, Front. Astron. Space Sci. **6**, 043511 (2019).
[16] J. E. Kim, Weak-interaction singlet and strong CP invariance, Phys. Rev. Lett. **43**, 103 (1979).
[17] A. R. Zhitnitsky, On possible suppression of the axion hadron interactions (in Russian), Sov. J. Nucl. Phys. **31**, 260 (1980).
[18] M. Dine, W. Fischler, and M. Srednicki, A simple solution to the strong *CP* problem with a harmless axion, Phys. Lett. **104B**, 199 (1981).
[19] M. Shifman, A. Vainshtein, and V. Zakharov, Can confinement ensure natural *CP* invariance of strong interactions?, Nucl. Phys. **B166**, 493 (1980).
[20] M. Dine and W. Fischler, The not-so-harmless axion, Phys. Lett. **120B**, 137 (1983).
[21] N. Du *et al.* (ADMX Collaboration), Search for invisible axion dark matter with the axion dark matter experiment, Phys. Rev. Lett. **120**, 151301 (2018).
[22] T. Braine *et al.* (ADMX Collaboration), Extended search for the invisible axion with the axion dark matter experiment, Phys. Rev. Lett. **124**, 101303 (2020).
[23] C. Bartram *et al.* (ADMX Collaboration), Axion dark matter experiment: Run 1b analysis details, Phys. Rev. D **103**, 032002 (2021).
[24] C. Bartram *et al.* (ADMX Collaboration), Search for invisible axion dark matter in the 3.3–4.2 μeV mass range, Phys. Rev. Lett. **127**, 261803 (2021).
[25] A. K. Yi *et al.*, Axion dark matter search around 4.55 μeV with Dine-Fischler-Srednicki-Zhitnitskii sensitivity, Phys. Rev. Lett. **130**, 071002 (2023).
[26] D. Kim, J. Jeong, S. Youn, Y. Kim, and Y. K. Semertzidis, Revisiting the detection rate for axion haloscopes, J. Cosmol. Astropart. Phys. 03 (2020) 066.
[27] A. Quiskamp, B. T. McAllister, P. Altin, E. N. Ivanov, M. Goryachev, and M. E. Tobar, Direct search for dark matter axions excluding alp cogenesis in the 63- to 67-μeV range with the organ experiment, Sci. Adv. **8**, eabq3765 (2022).
[28] B. T. McAllister, G. Flower, E. N. Ivanov, M. Goryachev, J. Bourhill, and M. E. Tobar, The organ experiment: An axion haloscope above 15 GHz, Phys. Dark Universe **18**, 67 (2017).
[29] R. T. Co, L. J. Hall, and K. Harigaya, Predictions for axion couplings from ALP cogenesis, J. High Energy Phys. 01 (2021) 172.
[30] R. T. Co, L. J. Hall, and K. Harigaya, Axion kinetic misalignment mechanism, Phys. Rev. Lett. **124**, 251802 (2020).
[31] R. T. Co and K. Harigaya, Axiogenesis, Phys. Rev. Lett. **124**, 111602 (2020).
[32] R. H. Dicke, The measurement of thermal radiation at microwave frequencies, Rev. Sci. Instrum. **17**, 268 (2004).
[33] M. Xu, X. Han, C.-L. Zou, W. Fu, Y. Xu, C. Zhong, L. Jiang, and H. X. Tang, Radiative cooling of a superconducting resonator, Phys. Rev. Lett. **124**, 033602 (2020).
[34] I. H. Rodrigues, D. Niepce, A. Pourkabirian, G. Moschetti, J. Schleeh, T. Bauch, and J. Grahn, On the angular dependence of InP high electron mobility transistors for cryogenic low noise amplifiers in a magnetic field, AIP Adv. **9**, 085004 (2019).
[35] J. Jeong, S. Youn, and J. E. Kim, Multiple-cell cavity design for high mass axion searches: An extended study, Nucl. Instrum. Methods Phys. Res., Sect. A **1053**, 168327 (2023).
[36] A. P. Quiskamp, B. T. Mcallister, G. Rybka, and M. E. Tobar, Dielectric-boosted sensitivity to cylindrical azimuthally varying transverse-magnetic resonant modes in an axion haloscope, Phys. Rev. Appl. **14**, 044051 (2020).
[37] B. T. McAllister, G. Flower, L. E. Tobar, and M. E. Tobar, Tunable supermode dielectric resonators for axion dark-matter haloscopes, Phys. Rev. Appl. **9**, 014028 (2018).
[38] A. Caldwell, G. Dvali, B. Majorovits, A. Millar, G. Raffelt, J. Redondo, O. Reimann, F. Simon, and F. Steffen (MADMAX Working Group), Dielectric haloscopes: A new way to detect axion dark matter, Phys. Rev. Lett. **118**, 091801 (2017).
[39] R. Cervantes, G. Carosi, S. Kimes, C. Hanretty, B. H. LaRoque, G. Leum, P. Mohapatra, N. S. Oblath, R. Ottens, Y. Park, G. Rybka, J. Sinnis, and J. Yang, ADMX-Orpheus first search for 70 μeV dark photon dark matter: Detailed design, operations, and analysis, Phys. Rev. D **106**, 102002 (2022).
[40] B. T. McAllister, A. P. Quiskamp, and M. E. Tobar, companion paper, Tunable rectangular resonant cavities for axion haloscopes, Phys. Rev. D **109**, 015013 (2024).
[41] B. M. Brubaker, L. Zhong, S. K. Lamoreaux, K. W. Lehnert, and K. A. V. Bibber, HAYSTAC axion search analysis procedure, Phys. Rev. D **96**, 123008 (2017).
[42] V. Anastassopoulos *et al.* (CAST Collaboration), New cast limit on the axion-photon interaction, Nat. Phys. **13**, 584 (2017).
[43] D. Alesini, C. Braggio, G. Carugno, N. Crescini, D. D'Agostino, D. Di Gioacchino, R. Di Vora, P. Falferi, U. Gambardella, C. Gatti, G. Iannone, C. Ligi, A. Lombardi, G. Maccarrone, A. Ortolan, R. Pengo, A. Rettaroli, G. Ruoso, L. Taffarello, and S. Tocci, Search for invisible axion dark matter of mass $m_a = 43$ μeV with the QUAX–$a\gamma$ experiment, Phys. Rev. D **103**, 102004 (2021).